

Topological Phases in Non-Hermitian Nonlinear-Eigenvalue Systems

Yu-Peng Ma^①,¹ Ming-Jian Gao^①,¹ and Jun-Hong An^{①, *}

¹*Key Laboratory of Quantum Theory and Applications of Ministry of Education, Lanzhou Center for Theoretical Physics, Gansu Provincial Research Center for Basic Disciplines of Quantum Physics, Key Laboratory of Theoretical Physics of Gansu Province, Lanzhou University, Lanzhou 730000, China*

The discovery of topological phases has ushered in a new era of condensed matter physics and revealed a variety of natural and artificial materials. They obey the bulk–boundary correspondence (BBC), which guarantees the emergence of boundary states with non-zero topological invariants in the bulk. A wide attention has been paid to extending topological phases to nonlinear and non-Hermitian systems. However, the BBC and topological invariants of non-Hermitian nonlinear systems remain largely unexplored. Here, we establish a complete BBC and topological characterization of the topological phases in a class of non-Hermitian nonlinear-eigenvalue systems by introducing an auxiliary system. We restore the BBC broken by non-Hermiticity via employing the generalized Brillouin zone on the auxiliary system. Remarkably, we discover that the interplay between non-Hermiticity and nonlinearity creates an exotic complex-band topological phase that coexists with the real-band topological phase. Our results enrich the family of nonlinear topological phases and lay a foundation for exploring novel topological physics in metamaterial systems.

Introduction.—The rapid development of topological insulators and superconductors has triggered a revolution in condensed matter physics and unlocked diverse advanced functionalities in natural and artificial materials [1–5]. Going beyond Landau’s phase transition paradigm, they are not caused by the breaking of symmetries [6, 7]. Their common feature is the presence of boundary states in the bulk gap, which are protected by symmetries and robust to disorder. What lies at the heart of them is the bulk-boundary correspondence (BBC). It indicates that these boundary states are intrinsically guaranteed by the topology of the bulk bands of systems [8–14]. Depending on different symmetries satisfied by the bulk bands, topological phases are classified into various categories [4, 8, 15]. This classification rule has not only guided the discovery of rich topological phases of matter in different electronic materials [16–18], but also the simulation of these phases on multiple platforms, including photonics [19–22], circuit [23–25], ultracold atom [26–28], and acoustic [29–32] systems.

Widespread interest has been attracted in topological phases of nonlinear systems. People desire to understand how to generalize the well developed BBC and topological characterization from linear to nonlinear systems. There are two types of nonlinear systems. The first type is the widely studied nonlinear-eigenvector systems. It emerges naturally in topological photonics in the presence of Kerr effect [33–37], topoelectric circuits by adding nonlinear electronic components [38–40], and mechanical metamaterials of masses connected by nonlinear springs [41]. The impact of nonlinearity on boundary states gives rise to unique topological phenomena intertwined with soliton [42–48] and synchronization [49–51], and a potential realization of high-performance topological lasers [52]. The BBC of the topological phases in this type of nonlinear systems has been constructed by directly defining topological invariants on the nonlinear eigenvectors

[35, 53]. The second type is the less explored nonlinear-eigenvalue systems [54]. It occurs in photonic systems in the medium with frequency-dependent permittivity [55–62], in elastic metamaterials [63], and quantum open and many-body systems [64, 65]. It has been found that the topological phases of this type of systems cannot be uniquely determined by the Hamiltonian alone. Furthermore, their eigenvalues may become complex even in the Hermitian case. They make the exploration of the BBC and topological characterization of their topological phases troublesome. Only recently, a method was proposed to reveal the BBC of the real-band topological phases of a nonlinear-eigenvalue system by mapping the system to an auxiliary linear system [66]. However, an open question remains regarding nonlinear-eigenvalue systems with topological phases, particularly photonic systems, which typically possess non-Hermiticity caused by optical gain, loss, and non-reciprocity effects [52, 67]. This non-Hermiticity can lead to a breakdown of the BBC [68–72]. Thus, it is highly desirable to solve the problem of how to characterize the non-Hermitian topological phases in nonlinear-eigenvalue systems.

Here, we investigate the topological phase transition of a class of non-Hermitian nonlinear-eigenvalue systems with second- and third-order nonlinearities. By using the auxiliary-system method, a complete BBC and topological characterization of the non-Hermitian topological phases in such nonlinear systems are established. A non-Bloch band theory is developed to describe the non-Hermitian topological phases with nonlinear eigenvalues by introducing the generalized Brillouin zone on the auxiliary system. Importantly, we find that an exotic topological phase with coexisting real- and complex-band boundary states emerges in our non-Hermitian nonlinear-eigenvalue system. Our result serves as a useful tool for investigating the rich topological phases in non-Hermitian nonlinear-eigenvalue systems.

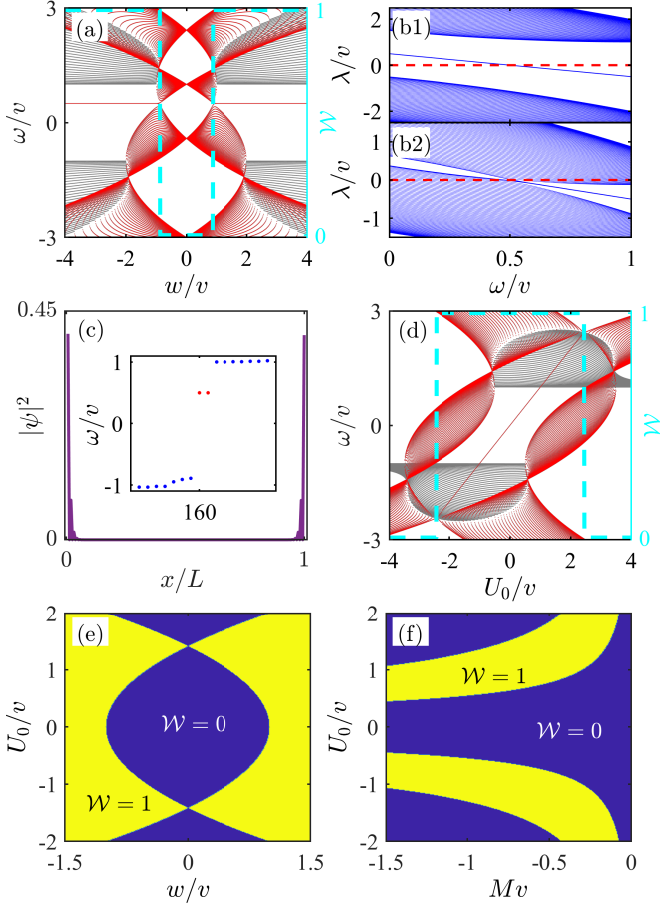


Figure 1. (a) Real- ω bands (red lines), real part of complex- ω bands (gray lines), and winding number \mathcal{W} (cyan dashed lines) in different w . Band structure of λ when (b1) $w = 2v$ and (b2) $0.875v$. (c) Probability distribution of the edge states, with the inset being the eigenvalues. (d) Real- ω bands (red lines), real part of complex- ω bands (gray lines), and \mathcal{W} in different U_0 when $w = 2v$. (e) Phase diagrams in the (e) U_0 - w and (f) U_0 - M spaces when $w = 0.75v$. We use $U_0 = 0.5v$ in (a)-(c) and $M = -0.5v^{-1}$ and $L = 80$ for all.

Topological phases in Hermitian nonlinear systems.—First, we consider a system satisfying a Hermitian nonlinear-eigenvalue equation

$$H_0 |\psi\rangle = \omega \mathcal{S}(\omega) |\psi\rangle, \quad (1)$$

where H_0 is a Hermitian Hamiltonian matrix, $\mathcal{S}(\omega)$ is called the overlap matrix, and ω is the nonlinear eigenvalue. The presence of ω -dependent $\mathcal{S}(\omega)$ makes the system nonlinear. Equation (1) can describe the light propagation in photonic crystals, where the frequency dependence of permittivity results in the presence of $\mathcal{S}(\omega)$ [55–62]. The nonlinearity renders some of the eigenvalues ω to be complex even when H_0 is Hermitian [73]. The system may host the topological phases, which are defined in the band structure formed by all real ω [66, 74]. The topological phases in the nonlinear-eigenvalue system do

not obey the well-established BBC in linear systems. In order to establish their BBC, we introduce an auxiliary system whose eigen equation reads $P(\omega)|\phi\rangle = \lambda|\phi\rangle$ [56, 66, 75], where $P(\omega) = H_0 - \omega \mathcal{S}(\omega)$ is called the pencil matrix [76] and ω is treated as a free parameter. The eigenvalue λ of the pencil matrix has no physical meaning except for $\lambda = 0$, at which the original nonlinear-eigenvalue equation (1) is recovered. When the band structure of λ is topological, they possess gapless edge states under the OBC. These edge states cross $\lambda = 0$ so that they also emerge in the original system [66]. Thus, we can use the topological invariant defined in the auxiliary system to characterize the edge states and reveal the BBC of the original system.

Explicitly, we investigate a one-dimensional second-order nonlinear Su-Schrieffer-Heeger (SSH) model with $H_0 = \sum_{n=1}^L [U_0 c_n^\dagger c_n + (v c_{n,A}^\dagger c_{n,B} + \text{h.c.})] + \sum_{n=1}^{L-1} (w c_{n+1,A}^\dagger c_{n,B} + \text{h.c.})$ [77] and $\mathcal{S}(\omega) = s_0 + s_1 \omega$, with $s_0 = 1$ and $s_1 = -M \sum_{n=1}^L (c_{n,A}^\dagger c_{n,B} + \text{h.c.})$ [73]. Here, U_0 is the on-site potential, v and M are the linear and nonlinear intracell hopping rates, and w is the intercell hopping rate. Equation (1) can be rewritten in a formally linear form [78]

$$\begin{pmatrix} 0 & I \\ s_1^{-1} H_0 & -s_1^{-1} s_0 \end{pmatrix} \begin{pmatrix} |\psi\rangle \\ \omega |\psi\rangle \end{pmatrix} = \omega \begin{pmatrix} |\psi\rangle \\ \omega |\psi\rangle \end{pmatrix}. \quad (2)$$

By numerically solving Eq. (2), we obtain the four-band structure of ω under the OBC of the nonlinear system [see Fig. 1(a)]. It shows that the real part of the complex- ω bands do not contribute to a topological phase transition and the band touching of the real- ω bands results in the presence of the gaped edge states with an eigenvalue $\omega = U_0$. The band structure is recovered by the eigenvalue spectrum of λ of the auxiliary system under the OBC, where the gapless edge states cross $\lambda = 0$ just at $\omega = U_0$ [see Fig. 1(b1)]. Under the PBC, $P(\omega)$ is converted into the momentum-space form $P(k, \omega) = \sum_{j=0, \pm} p_j(k, \omega) \sigma_j$, where σ_0 is the identity matrix, $\sigma_{\pm} = (\sigma_x \pm i\sigma_y)/2$, $p_0(k, \omega) = U_0 - \omega$, and $p_{\pm}(k, \omega) = v + M\omega^2 + we^{\mp ik}$. It is easily obtained from $P(k, \omega)$ that, at the high-symmetry points $k = 0$ and π , the bulk bands touch at $\omega = U_0$ when $MU_0^2 + v = \pm w$, which gives the critical points of the topological phase transition. These critical points match the ones obtained under the OBC, where the bands across $\lambda = 0$ touch together just at $\omega = U_0$ [see Fig. 1(b2)]. Such a matching firmly establishes the BBC of the original nonlinear system. $P(k, U_0)$ satisfies time-reversal symmetry $\mathcal{T}P(k, U_0)\mathcal{T}^{-1} = P(-k, U_0)$, chiral symmetry $\Gamma P(k, U_0)\Gamma^{-1} = -P(k, U_0)$, and particle-hole symmetry $\mathcal{C}P(k, U_0)\mathcal{C}^{-1} = -P(-k, U_0)$, with \mathcal{T} being the complex conjugation, $\Gamma = \sigma_z$, and $\mathcal{C} = \sigma_z \mathcal{K}$. Thus, the edge states exhibit the twofold Kramers degeneracy [see Fig. 1(c)]

and the topology is well described by the winding number

$$\mathcal{W} = \frac{1}{2\pi i} \int_{-\pi}^{\pi} dk \frac{d}{dk} \ln p_-(k, U_0). \quad (3)$$

It is easy to find $\mathcal{W} = 1$ when $|MU_0^2 + v| < |w|$.

We see from Fig. 1(a) that \mathcal{W} defined in the auxiliary system correctly characterizes the topological phases of the original nonlinear system. Due to the nonlinearity, the on-site potential U_0 also plays a dominant role in triggering the topological phase transition, which is very different from linear systems. Figure 1(d) displays the band structure of ω under the OBC in different U_0 when $w = 2v$. Being similar to Fig. 1(a), the complex- ω bands do not contribute any topological phase transition. The twofold degenerate edge states with $\omega = U_0$ are present in the real- ω bands when $U_0^2 < -(w+v)/M$. They are well characterized by the winding number \mathcal{W} defined in $P(k, U_0)$. To gain a global picture, we plot in Figs. 1(e) and 1(f) the phase diagrams in the U_0 - w and U_0 - M spaces. Figure 1(f) demonstrates the nonlinearity term M can drive the topologically trivial linear system with $M = 0$ to a topological phase. It indicates that the nonlinearity supplies us an extra dimension to engineer the topological phases. Thus, we have established a complete topological characterization and the BBC for the Hermitian topological phases in the nonlinear-eigenvalue system, where the system topology is contributed by real bands. Next, we investigate the cases where non-Hermiticity is present in the Hamiltonian matrix and the overlap matrix, respectively.

Real-band topological phases in non-Hermitian nonlinear systems.—Consider that the non-Hermitian terms induced by the non-reciprocal hoppings are present in the Hamiltonian matrix as

$$H = H_0 + \delta \sum_{n=1}^L (c_{n,A}^\dagger c_{n,B} - c_{n,B}^\dagger c_{n,A}), \quad (4)$$

where δ is a non-reciprocal parameter between the two directions of the intracell hopping rates [71]. The overlap matrix $\mathcal{S}(\omega)$ takes the same form as the one in the preceding section. The momentum-space pencil matrix of the associated auxiliary system under the PBC becomes $P(k, \omega) = \sum_{j=0, \pm} p_j(k, \omega) \sigma_j$, where $p_0(k, \omega) = U_0 - \omega$ and $p_{\pm}(k, \omega) = M\omega^2 + v + we^{\mp ik} \pm \delta$. It is easy to see that, at the two high-symmetry points $k = 0$ and π , the bands of $P(k, \omega)$ touch at $\omega = U_0$ when $MU_0^2 + v = w \pm \delta$ or $-w \pm \delta$. It is completely different from the band-touching condition $MU_0^2 + v = \pm\sqrt{w^2 + \delta^2}$ obtained under the OBC. This reflects the non-Hermiticity caused breakdown of BBC. In order to establish the BBC, we replace e^{ik} by $\beta = re^{ik}$ with $r = [(v + MU_0^2 - \delta)/(v + MU_0^2 + \delta)]^{1/2}$, which defines a generalized BZ [70]. Then $P(k, U_0)$ is converted into $\bar{P}(k, U_0) = \bar{p}_+(k, U_0)\sigma_+ + \bar{p}_-(k, U_0)\sigma_-$, with $\bar{p}_{\pm}(k, U_0) = MU_0^2 + v + w\beta^{\mp 1} \pm \delta$. It is remarkable to find that its

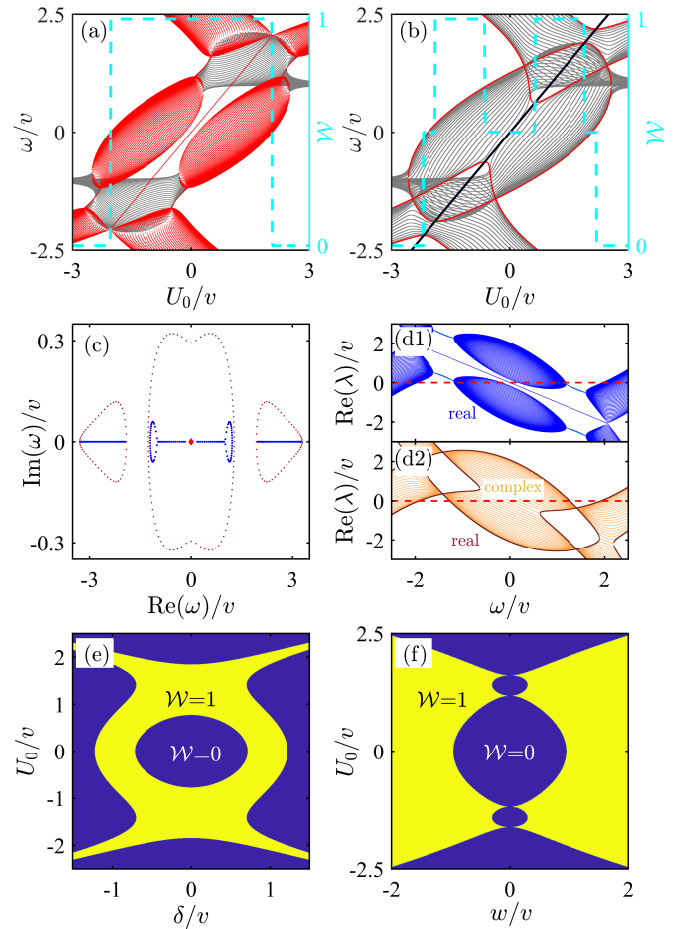


Figure 2. Real- ω bands (red lines), real part of complex- ω bands (gray lines) under the (a) OBC and (b) PBC. Winding numbers \mathcal{W} (cyan dashed lines) defined in the (a) generalized BZ and (b) BZ. The black solid line in (b) shows the Fermi level $\omega = U_0$. (c) Eigenvalues of λ . Band structures of $\text{Re}(\lambda)$ under (b1) the OBC (blue) and (b2) PBC (brown) when $U_0 = 0$. Phase diagrams in the (e) U_0 - δ and (f) U_0 - w spaces. We use $w = 1.1v$ in (a)-(d) and $0.75v$ in (e) and $\delta = 0.3v$, $M = -0.5v^{-1}$, and $L = 50$ for all.

band-touching condition successfully recovers the one under the OBC. In the similar manner as Eq. (3), we define the winding number of $\bar{P}(k, U_0)$ via the phase changes of $\bar{p}_{\pm}(k, U_0)$ when k runs over the generalized BZ [71, 79, 80]

$$\mathcal{W} = \frac{1}{4\pi i} \int_{-\pi}^{\pi} dk \frac{d}{dk} \ln \frac{\bar{p}_-(k, U_0)}{\bar{p}_+(k, U_0)}. \quad (5)$$

We indeed find that $\mathcal{W} = 1$ and a pair of edge states is formed in both the auxiliary and original non-Hermitian systems when $|MU_0^2 + v| < \sqrt{w^2 + \delta^2}$.

Figure 2(a) shows the band structures of ω under the OBC in different U_0 obtained by numerically solving Eq. (2). Again, the topological phase transition is not contributed by the real part of the complex- ω bands, but by the real- ω bands. Accompanying the touching of the real- ω bands, the twofold degenerate edge states with

$\omega = U_0$ protected by the time-reversal symmetry are present when $U_0^2 < -[\sqrt{w^2 + \delta^2} + v]/M$. This band structure is dramatically different from the one under the PBC [see Fig. 2(b)], where the real- ω bands touch the Fermi level $\omega = U_0$ at $U_0^2 = (w - \delta - v)/M$ or $(-w \pm \delta - v)/M$, while the bands of the real part of the complex ω are closed at almost all the positions where the edge states are present in Fig. 2(a). We further plot in Fig. 2(c) all the eigenvalues of ω when $U_0 = 0$. It confirms that the bands in the presence of the edge state under the OBC are closed under the PBC. The mismatching of the bulk band structures under these two boundary conditions clearly demonstrates the breakdown of the BBC caused by the non-Hermiticity. The two real- λ band structures can be recovered by $\text{Re}(\lambda)$ of the auxiliary system under the corresponding boundary conditions in Fig. 2(d1) for OBC and Fig. 2(d2) for PBC. The gapless edge states in the $\text{Re}(\lambda)$ -bands under the OBC cross $\lambda = 0$ precisely at $\omega = U_0$, which is consistent with Fig. 2(a). However, the $\text{Re}(\lambda)$ bands under the PBC across $\lambda = 0$ do not exhibit a gap. It verifies the breakdown of the BBC. The winding number of $P(k, U_0)$ calculated in the conventional BZ is given in Fig. 2(b). Although qualitatively capturing the touching points of the real ω and the Fermi level U_0 under the PBC, the winding numbers defined in the conventional BZ nonphysically take half integers. Importantly, it cannot characterize the edge states under the OBC. However, the one defined in $\bar{p}_\pm(k, U_0)$ of the generalized BZ correctly counts the pair number of the edge states [see Fig. 2(a)]. We thus establish a non-Bloch BBC for our nonlinear system. Figures 2(e) and 2(f) show the phase diagrams characterized by \mathcal{W} in the U_0 - δ and U_0 - w spaces. They give a global picture of the topological phases in the non-Hermitian nonlinear system.

We have discovered in this case that non-Hermiticity leads to the breakdown of the BBC in nonlinear eigenvalue systems. Due to the topological inheritance of the original system by the auxiliary system under OBC, we can introduce a generalized BZ in the auxiliary system to restore the BBC. However, this still falls within the realm of real-band topology. Next, we will examine the scenario where non-Hermiticity is present in the overlap matrix such that the topological phases coexist in both the real and complex bands.

Complex-band topological phases in non-Hermitian nonlinear systems.—We study a third-order nonlinear non-Hermitian SSH model. It possesses the same Hermitian Hamiltonian matrix H_0 as the preceding sections and a non-Hermitian overlap matrix $\mathcal{S}(\omega) = s_0 + \tilde{s}_1\omega + \tilde{s}_2\omega^2$, where $s_0 = 1$, $\tilde{s}_1 = -\gamma \sum_{n=1}^L (c_{n,A}^\dagger c_{n,B} - c_{n,B}^\dagger c_{n,A})$ and $\tilde{s}_2 = -i\mathcal{M}$ [70, 73]. Here, γ is a non-reciprocal parameter between the two directions of the nonlinear intracell hopping rates and \mathcal{M} is the nonlinear loss-gain parameter.

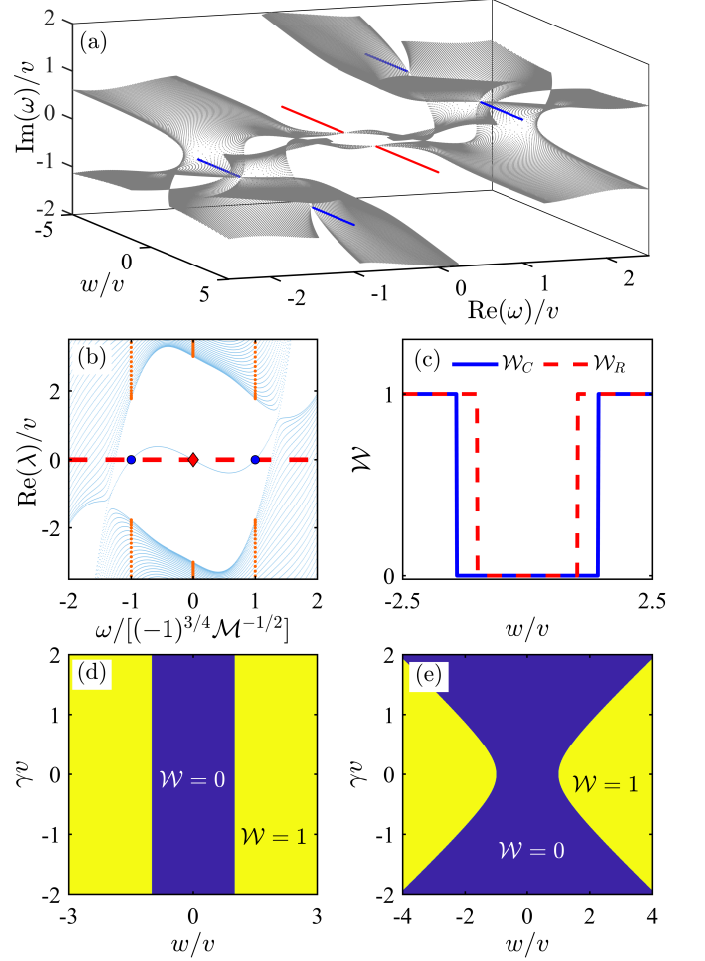


Figure 3. (a) Band structure of ω in different w . The real and complex edge-mode eigenvalues are marked by red and blue lines, respectively. (b) Band structures of the real part of complex λ (blue dots) and real λ (orange dots) when $w = 4v$. (c) Winding numbers in different w . Phase diagrams for the real (d) and complex (e) edge modes. We use $\mathcal{M} = -0.5v^{-2}$, $\gamma = v^{-1}$, and $L = 100$.

Equation (1) is formally rewritten as [78]

$$\begin{pmatrix} 0 & I & 0 \\ 0 & 0 & I \\ \tilde{s}_2^{-1} H_0 & -\tilde{s}_2^{-1} s_0 & -\tilde{s}_2^{-1} \tilde{s}_1 \end{pmatrix} \begin{pmatrix} |\psi\rangle \\ \omega|\psi\rangle \\ \omega^2|\psi\rangle \end{pmatrix} = \omega \begin{pmatrix} |\psi\rangle \\ \omega|\psi\rangle \\ \omega^2|\psi\rangle \end{pmatrix}. \quad (6)$$

It shows that the presence of \tilde{s}_2 turns the system into a six-band model. The momentum-space pencil matrix of the auxiliary system is derived to be $P(k, \omega) = \sum_{j=0, \pm} p_j(k, \omega) \sigma_j$, where $p_0(k, \omega) = i\mathcal{M}\omega^3 - \omega$ and $p_{\pm}(k, \omega) = v \pm \gamma\omega^2 + we^{\mp ik}$. $P(k, \omega)$ satisfies the chiral symmetry $\Gamma P(k, \omega) \Gamma^{-1} = -P(k, -\omega)$. Its bands touch under the condition $i\mathcal{M}\omega^3 - \omega = 0$, whose solutions are $\omega = 0$ and $\pm(-1)^{3/4} \mathcal{M}^{-1/2}$. Therefore, the system may host both the real edge modes at $\omega = 0$ and the complex edge modes at $\omega = \pm(-1)^{3/4} \mathcal{M}^{-1/2}$. For the real edge

modes at $\omega = 0$, the pencil matrix reduces to $P_R(k, 0) = (v + we^{-ik})\sigma_+ + \text{H.c.}$, which is just a linear SSH model. At the high-symmetry points $k = 0$ and π , the real bands of $P_R(k, 0)$ touch at $|v| = |w|$. The pencil matrix for the complex edge modes at $\omega = \pm(-1)^{3/4}\mathcal{M}^{-1/2}$ becomes $P_C(k, \pm(-1)^{3/4}\mathcal{M}^{-1/2}) = (v - \frac{i\gamma}{\mathcal{M}} + we^{-ik})\sigma_+ + \text{H.c.}$, whose bands touch at $|k| = |\arccos[\pm v/\sqrt{(\gamma/\mathcal{M})^2 + v^2}]|$ when $w^2 = (\gamma/\mathcal{M})^2 + v^2$. It is interesting to find that, although the overlap matrix contains non-Hermitian term and the edges modes possess complex eigenvalues, the pencil matrix of the associated auxiliary system is Hermitian. Therefore, it is naturally expected that the original and the auxiliary systems obey the BBC. The winding numbers for the real and complex bands can be defined in $P_R(k, 0)$ and $P_C(k, \pm(-1)^{3/4}\mathcal{M}^{-1/2})$ in a manner similar to that of the Hermitian case.

By numerically solving Eq. (6), we obtain the complex- ω bands under the OBC in different w [see Fig. 3(a)]. It is remarkable to find that the gapped edge states have not only a real eigenvalue $\omega = 0$ (red lines) but also two complex eigenvalues $\omega = \pm(-1)^{3/4}\mathcal{M}^{-1/2}$ (blue lines). The former ones with $\omega = 0$ are present when $|w| > |v|$. The latter ones with $\omega = \pm(-1)^{3/4}\mathcal{M}^{-1/2}$ are present when $w^2 > (\gamma/\mathcal{M})^2 + v^2$. Figure 3(b) shows the λ band of the auxiliary system under the OBC. It clearly indicates that a gapless complex edge mode intersects with $\lambda = 0$ just at $\omega = 0$ and $\pm(-1)^{3/4}\mathcal{M}^{-1/2}$, corresponding exactly to the two types of edge modes in Fig. 3(a). The orange points in the bulk bands reveal that all the values of λ are real, whose positions exactly match $\omega = 0$ and $\pm(-1)^{3/4}\mathcal{M}^{-1/2}$. Therefore, the auxiliary system at these three positions is Hermitian and we can calculate the topological numbers defined in the pencil matrices $P_R(k, 0)$ and $P_C(k, \pm(-1)^{3/4}\mathcal{M}^{-1/2})$ to characterize the real and complex edge modes, respectively. The obtained winding numbers correctly count the pair number of the two types of edge states [see Fig. 3(c)]. The phase diagrams for the real and complex edge bands in the γ - w space are depicted in Figs. 3(e) and 3(d). They give a global picture on the non-Hermitian topological phases of this third-order nonlinear-eigenvalue system. To the best of our knowledge, such a topological phase in the complex bands has never been reported before.

Discussion and Conclusion.—Nonlinear-eigenvalue problems arise in various physical systems. For example, in the study of higher-order nonlinear responses of graphene [61, 81, 82], the wave propagation problem is reduced to an eigenvalue problem. Additionally, when analyzing waveguide filter structures with frequency-dependent material properties or specific boundary conditions, their permittivity or permeability becomes frequency-dependent rather than constant [55–62]. Consequently, the analysis of their resonant characteristics can be formulated as a nonlinear-eigenvalue problem. Meanwhile, waveguide arrays can also be employed to simulate topological insulators [83, 84], including

non-Hermitian topological insulators [85–87]. In the field of structural acoustics, its dynamic equation takes the form of a quadratic nonlinear-eigenvalue problem [88]. Furthermore, acoustic systems can be used similarly to model topological insulators [89–93]. Therefore, our system can be conceptually derived from the design principles of these practical systems.

We have investigated the non-Hermitian topological phases in the nonlinear-eigenvalue system. A complete topological characterization has been established by introducing an auxiliary system. It is remarkable to find that, in addition to the conventional non-Hermitian topological phases in the real bands, exotic complex-band non-Hermitian topological phases are present in the system. In the case that the nonreciprocal hoppings in the Hamiltonian matrix break the BBC of the real-band topological phases, we have succeeded in restoring the BBC via introducing the generalized BZ in the auxiliary system. When the nonreciprocal hoppings are present in the overlap matrix, coexisting complex- and real-band topological phases are discovered. Although processing a complex eigenvalue, the complex-band topological phases correspond to a Hermitian Hamiltonian of the auxiliary system. This enables us to apply the well established characterization in the Hermitian system to describe the complex-band topological phases. Enriching the family of nonlinear topological phases, our result lays a foundation for exploring novel nonlinear topological phases, especially in optical, acoustic, and elastic metamaterial systems.

Acknowledgments.—The work is supported by the National Natural Science Foundation of China (Grants No. 124B2090, No. 12275109, No. 92576202, and No. 12247101), the Quantum Science and Technology-National Science and Technology Major Project (Grant No. 2023ZD0300904), the Fundamental Research Funds for the Central Universities (Grant No. lzujbky-2025-jdzx07), and the Natural Science Foundation of Gansu Province (No. 22JR5RA389 and No. 25JRRRA799).

* anjhong@lzu.edu.cn

- [1] M. Z. Hasan and C. L. Kane, Colloquium: Topological insulators, *Rev. Mod. Phys.* **82**, 3045 (2010).
- [2] X.-L. Qi and S.-C. Zhang, Topological insulators and superconductors, *Rev. Mod. Phys.* **83**, 1057 (2011).
- [3] A. Bansil, H. Lin, and T. Das, Colloquium: Topological band theory, *Rev. Mod. Phys.* **88**, 021004 (2016).
- [4] C.-K. Chiu, J. C. Y. Teo, A. P. Schnyder, and S. Ryu, Classification of topological quantum matter with symmetries, *Rev. Mod. Phys.* **88**, 035005 (2016).
- [5] F. D. M. Haldane, Nobel lecture: Topological quantum matter, *Rev. Mod. Phys.* **89**, 040502 (2017).
- [6] C. L. Kane and E. J. Mele, Quantum Spin Hall Effect in Graphene, *Phys. Rev. Lett.* **95**, 226801 (2005).
- [7] C. L. Kane and E. J. Mele, Z_2 Topological Order and the

Quantum Spin Hall Effect, *Phys. Rev. Lett.* **95**, 146802 (2005).

[8] A. P. Schnyder, S. Ryu, A. Furusaki, and A. W. W. Ludwig, Classification of topological insulators and superconductors in three spatial dimensions, *Phys. Rev. B* **78**, 195125 (2008).

[9] L. Fu and C. L. Kane, Topological insulators with inversion symmetry, *Phys. Rev. B* **76**, 045302 (2007).

[10] D. Nakamura, T. Bessho, and M. Sato, Bulk-Boundary Correspondence in Point-Gap Topological Phases, *Phys. Rev. Lett.* **132**, 136401 (2024).

[11] J. Zhu, Y. Feng, X. Zhou, Y. Wang, H. Yao, Z. Lian, W. Lin, Q. He, Y. Lin, Y. Wang, Y. Wang, S. Yang, H. Li, Y. Wu, C. Liu, J. Wang, J. Shen, J. Zhang, Y. Wang, and Y. Wang, Direct observation of chiral edge current at zero magnetic field in a magnetic topological insulator, *Nature Communications* **16**, 963 (2025).

[12] C. Li, R. Wang, S. Zhang, Y. Qin, Z. Ying, B. Wei, Z. Dai, F. Guo, W. Chen, R. Zhang, B. Wang, X. Wang, and F. Song, Observation of giant non-reciprocal charge transport from quantum Hall states in a topological insulator, *Nature Materials* **23**, 1208 (2024).

[13] M. S. Hossain, Q. Zhang, Z. Wang, N. Dhale, W. Liu, M. Litskevich, B. Casas, N. Shumiya, J.-X. Yin, T. A. Cochran, Y. Li, Y.-X. Jiang, Y. Zhang, G. Cheng, Z.-J. Cheng, X. P. Yang, N. Yao, T. Neupert, L. Balicas, Y. Yao, B. Lv, and M. Z. Hasan, Quantum transport response of topological hinge modes, *Nature Physics* **20**, 776 (2024).

[14] S. Yu, J. Deng, W. Liu, Y. Zhang, Y. Sun, N. Dhale, S. Li, W. Ma, Z. Wang, P. Wu, Z. Liang, X. Zhang, B. Lv, Z. Wang, Z. Wang, and X. Chen, Observation of Robust One-Dimensional Edge Channels in a Three-Dimensional Quantum Spin Hall Insulator, *Phys. Rev. X* **14**, 041048 (2024).

[15] R. Takahashi and T. Ozawa, Bulk-entanglement spectrum correspondence in PT - and PC -symmetric topological insulators and superconductors, *Phys. Rev. Res.* **6**, 033192 (2024).

[16] C. Zhang, X. Lu, N. Wang, T. Huang, H. Zhang, N. Cao, A. Wang, X. Zhou, K. Watanabe, T. Taniguchi, S.-Y. Xu, and W. Gao, Zero-field chiral edge transport in an intrinsic magnetic topological insulator mnb2te4, *Nature Communications* **16**, 5587 (2025).

[17] H. Yi, Y.-F. Zhao, Y.-T. Chan, J. Cai, R. Mei, X. Wu, Z.-J. Yan, L.-J. Zhou, R. Zhang, Z. Wang, S. Paolini, R. Xiao, K. Wang, A. R. Richardella, J. Singleton, L. E. Winter, T. Prokscha, Z. Salman, A. Suter, P. P. Balakrishnan, A. J. Grutter, M. H. W. Chan, N. Samarth, X. Xu, W. Wu, C.-X. Liu, and C.-Z. Chang, Interface-induced superconductivity in magnetic topological insulators, *Science* **383**, 634 (2024).

[18] K. Huang, H. Fu, K. Watanabe, T. Taniguchi, and J. Zhu, High-temperature quantum valley hall effect with quantized resistance and a topological switch, *Science* **385**, 657 (2024).

[19] L. Lu, J. D. Joannopoulos, and M. Soljačić, Topological photonics, *Nature photonics* **8**, 821 (2014).

[20] L. Huang, L. He, W. Zhang, H. Zhang, D. Liu, X. Feng, F. Liu, K. Cui, Y. Huang, W. Zhang, and X. Zhang, Hyperbolic photonic topological insulators, *Nature Communications* **15**, 1647 (2024).

[21] G.-G. Liu, S. Mandal, X. Xi, Q. Wang, C. Devescovi, A. Morales-Pérez, Z. Wang, L. Yang, R. Banerjee, Y. Long, Y. Meng, P. Zhou, Z. Gao, Y. Chong, A. García-Etxarri, M. G. Vergniory, and B. Zhang, Photonic axion insulator, *Science* **387**, 162 (2025).

[22] S. Mandal, Z. Wang, R. Banerjee, H. T. Teo, M. Wei, P. Zhou, X. Xi, Z. Gao, G.-G. Liu, and B. Zhang, Photonic Bilayer Chern Insulator with Corner States, *Phys. Rev. Lett.* **135**, 016903 (2025).

[23] J. Ningyuan, C. Owens, A. Sommer, D. Schuster, and J. Simon, Time- and site-resolved dynamics in a topological circuit, *Phys. Rev. X* **5**, 021031 (2015).

[24] P. M. Lenggenhager, A. Stegmaier, L. K. Upreti, T. Hofmann, T. Helbig, A. Vollhardt, M. Greiter, C. H. Lee, S. Imhof, H. Brand, T. Kießling, I. Boettcher, T. Neupert, R. Thomale, and T. Bzdušek, Simulating hyperbolic space on a circuit board, *Nature Communications* **13**, 4373 (2022).

[25] Y. Wang, H. M. Price, B. Zhang, and Y. D. Chong, Circuit implementation of a four-dimensional topological insulator, *Nature Communications* **11**, 2356 (2020).

[26] G. Jotzu, M. Messer, R. Desbuquois, M. Lebrat, T. Uehlinger, D. Greif, and T. Esslinger, Experimental realization of the topological haldane model with ultracold fermions, *Nature* **515**, 237 (2014).

[27] J. Fraxanet, A. Dauphin, M. Lewenstein, L. Barbiero, and D. González-Cuadra, Higher-Order Topological Peierls Insulator in a Two-Dimensional Atom-Cavity System, *Phys. Rev. Lett.* **131**, 263001 (2023).

[28] C. Braun, R. Saint-Jalm, A. Hesse, J. Arceri, I. Bloch, and M. Aidelsburger, Real-space detection and manipulation of topological edge modes with ultracold atoms, *Nature Physics* **20**, 1306 (2024).

[29] C. L. Kane and T. C. Lubensky, Topological boundary modes in isostatic lattices, *Nature Physics* **10**, 39 (2014).

[30] H. Xue, Y. Yang, F. Gao, Y. Chong, and B. Zhang, Acoustic higher-order topological insulator on a kagome lattice, *Nature Materials* **18**, 108 (2019).

[31] Z. Cheng, S. Yue, Y. Long, W. Xie, Z. Yu, H. T. Teo, Y. X. Zhao, H. Xue, and B. Zhang, Observation of returning Thouless pumping, *Nature Communications* **16**, 9669 (2025).

[32] X.-C. Sun, J.-B. Wang, C. He, and Y.-F. Chen, Non-Abelian Topological Phases and Their Quotient Relations in Acoustic Systems, *Phys. Rev. Lett.* **132**, 216602 (2024).

[33] D. Leykam and Y. D. Chong, Edge solitons in nonlinear-photonic topological insulators, *Phys. Rev. Lett.* **117**, 143901 (2016).

[34] D. Smirnova, D. Leykam, Y. Chong, and Y. Kivshar, Nonlinear topological photonics, *Applied Physics Reviews* **7**, 021306 (2020).

[35] K. Sone, M. Ezawa, Y. Ashida, N. Yoshioka, and T. Sagawa, Nonlinearity-induced topological phase transition characterized by the nonlinear Chern number, *Nature Physics* **20**, 1164 (2024).

[36] A. Szameit and M. C. Rechtsman, Discrete nonlinear topological photonics, *Nature Physics* **20**, 905 (2024).

[37] S. Ravets, N. Pernet, N. Mostaan, N. Goldman, and J. Bloch, Thouless Pumping in a Driven-Dissipative Kerr Resonator Array, *Phys. Rev. Lett.* **134**, 093801 (2025).

[38] Y. Hadad, J. C. Soric, A. B. Khanikaev, and A. Alù, Self-induced topological protection in nonlinear circuit arrays, *Nature Electronics* **1**, 178 (2018).

[39] T. Kotwal, F. Moseley, A. Stegmaier, S. Imhof, H. Brand, T. Kießling, R. Thomale, H. Ronellenfitsch,

and J. Dunkel, Active topoelectrical circuits, *Proceedings of the National Academy of Sciences* **118**, e2106411118 (2021).

[40] H. Hohmann, T. Hofmann, T. Helbig, S. Imhof, H. Brand, L. K. Upreti, A. Stegmaier, A. Fritzsche, T. Müller, U. Schwingenschlögl, C. H. Lee, M. Greiter, L. W. Molenkamp, T. Kießling, and R. Thomale, Observation of cnoidal wave localization in nonlinear topoelectric circuits, *Phys. Rev. Res.* **5**, L012041 (2023).

[41] R. Chaunsali and G. Theocharis, Self-induced topological transition in phononic crystals by nonlinearity management, *Phys. Rev. B* **100**, 014302 (2019).

[42] Z. Wang, Y. D. Chong, J. D. Joannopoulos, and M. Soljačić, Reflection-Free One-way Edge Modes in a Gyromagnetic Photonic Crystal, *Phys. Rev. Lett.* **100**, 013905 (2008).

[43] Z. Zhang, R. Wang, Y. Zhang, Y. V. Kartashov, F. Li, H. Zhong, H. Guan, K. Gao, F. Li, Y. Zhang, and M. Xiao, Observation of edge solitons in photonic graphene, *Nature Communications* **11**, 1902 (2020).

[44] S. Mukherjee and M. C. Rechtsman, Observation of unidirectional solitonlike edge states in nonlinear floquet topological insulators, *Phys. Rev. X* **11**, 041057 (2021).

[45] Y. V. Kartashov, A. A. Arkhipova, S. A. Zhuravitskii, N. N. Skryabin, I. V. Dyakonov, A. A. Kalinkin, S. P. Kulik, V. O. Kompanets, S. V. Chekalin, L. Torner, and V. N. Zadkov, Observation of Edge Solitons in Topological Trimer Arrays, *Phys. Rev. Lett.* **128**, 093901 (2022).

[46] B. M. Manda, V. Achilleos, O. Richoux, C. Skokos, and G. Theocharis, Wave-packet spreading in the disordered and nonlinear Su-Schrieffer-Heeger chain, *Phys. Rev. B* **107**, 184313 (2023).

[47] J. W. Choi, B.-U. Sohn, H. Gao, G. F. R. Chen, J. S. Goh, D. K. T. Ng, and D. T. H. Tan, Observation of temporal optical solitons in a topological waveguide, *Scientific Reports* **14**, 28074 (2024).

[48] S. Coen, B. Garbin, G. Xu, L. Quinn, N. Goldman, G.-L. Oppo, M. Erkintalo, S. G. Murdoch, and J. Fatome, Nonlinear topological symmetry protection in a dissipative system, *Nature communications* **15**, 1398 (2024).

[49] K. Sone, Y. Ashida, and T. Sagawa, Topological synchronization of coupled nonlinear oscillators, *Phys. Rev. Res.* **4**, 023211 (2022).

[50] G. Moille, P. Shandilya, A. Niang, C. Menyuk, G. Carter, and K. Srinivasan, Versatile optical frequency division with kerr-induced synchronization at tunable microcomb synthetic dispersive waves, *Nature Photonics* **19**, 36 (2025).

[51] W. Zhang, F. Di, and X. Zhang, Non-Hermitian Global Synchronization, *Advanced Science* **12**, 2408460 (2025).

[52] C. R. Leefmans, M. Parto, J. Williams, G. H. Y. Li, A. Dutt, F. Nori, and A. Marandi, Topological temporally mode-locked laser, *Nature Physics* **20**, 852 (2024).

[53] S. Mukherjee and M. C. Rechtsman, Observation of Floquet solitons in a topological bandgap, *Science* **368**, 856 (2020).

[54] S. Güttel and F. Tisseur, The nonlinear eigenvalue problem, *Acta Numerica* **26**, 1–94 (2017).

[55] V. Kuzmiak, A. A. Maradudin, and F. Pincemin, Photonic band structures of two-dimensional systems containing metallic components, *Phys. Rev. B* **50**, 16835 (1994).

[56] S. Raghu and F. D. M. Haldane, Analogs of quantum-hall-effect edge states in photonic crystals, *Phys. Rev. A* **78**, 033834 (2008).

[57] P. Jorkowski and R. Schuhmann, Solving Nonlinear Eigenvalue Problems for Waveguide-Coupled Cavities Using an Integral Solver With Subspace Projection, *IEEE Transactions on Magnetics* **56**, 1 (2020).

[58] V. Lombardi, M. Bozzi, and L. Perregrini, A Novel Variational Meshless Method With Radial Basis Functions for Waveguide Eigenvalue Problems, *IEEE Transactions on Microwave Theory and Techniques* **66**, 3714 (2018).

[59] Z. Mai and Y. Y. Lu, Computing diffraction anomalies as nonlinear eigenvalue problems, *Phys. Rev. E* **106**, 035304 (2022).

[60] Q. Li, Q. Wu, S. Dou, J. Wang, S. Liu, and W. Chen, Nonlinear eigenvalue topology optimization for structures with frequency-dependent material properties, *Mechanical Systems and Signal Processing* **170**, 108835 (2022).

[61] Y. Smirnov and S. Tikhov, The Nonlinear Eigenvalue Problem of Electromagnetic Wave Propagation in a Dielectric Layer Covered with Graphene, *Photonics* **10**, 523 (2023).

[62] J. Bai, X. Bai, Z. Gao, and R. Yang, Frequency-dependent fundamental and dipole gap solitons in \mathcal{PT} -symmetric nonlinear metamaterials, *Phys. Rev. A* **109**, 043518 (2024).

[63] B. Vial, M. Martí Sabaté, R. Wiltshaw, S. Guenneau, and R. V. Craster, Quasinormal mode expansion in thin elastic plates, *Phys. Rev. B* **110**, 174305 (2024).

[64] S. Tanaka, S. Garmon, K. Kanki, and T. Petrosky, Higher-order time-symmetry-breaking phase transition due to meeting of an exceptional point and a fano resonance, *Phys. Rev. A* **94**, 022105 (2016).

[65] D. Li and E. Polizzi, Nonlinear eigenvalue algorithm for GW quasiparticle equations, *Phys. Rev. B* **111**, 045137 (2025).

[66] T. Isobe, T. Yoshida, and Y. Hatsugai, Bulk-Edge Correspondence for Nonlinear Eigenvalue Problems, *Phys. Rev. Lett.* **132**, 126601 (2024).

[67] K. Takata and M. Notomi, Photonic Topological Insulating Phase Induced Solely by Gain and Loss, *Phys. Rev. Lett.* **121**, 213902 (2018).

[68] T. E. Lee, Anomalous Edge State in a Non-Hermitian Lattice, *Phys. Rev. Lett.* **116**, 133903 (2016).

[69] H. Shen, B. Zhen, and L. Fu, Topological Band Theory for Non-Hermitian Hamiltonians, *Phys. Rev. Lett.* **120**, 146402 (2018).

[70] S. Yao and Z. Wang, Edge States and Topological Invariants of Non-Hermitian Systems, *Phys. Rev. Lett.* **121**, 086803 (2018).

[71] K. Yokomizo and S. Murakami, Non-Bloch Band Theory of Non-Hermitian Systems, *Phys. Rev. Lett.* **123**, 066404 (2019).

[72] N. Okuma, K. Kawabata, K. Shiozaki, and M. Sato, Topological Origin of Non-Hermitian Skin Effects, *Phys. Rev. Lett.* **124**, 086801 (2020).

[73] H. Li, A. Wang, and C. Q. Chen, Static topological lattices: Correspondence with tight-binding models, *Phys. Rev. B* **111**, 214107 (2025).

[74] S. Cheng, Y. Jiang, and G. Xianlong, Bulk-edge correspondence for the nonlinear eigenvalues problem of the Haldane model, *Phys. Rev. B* **109**, 134201 (2024).

[75] C. Bai and Z. Liang, Anomalous bulk-edge correspondence of the nonlinear rice-mele model, *Phys. Rev. A* **111**, 042201 (2025).

[76] K. D. Ikramov, Matrix pencils: Theory, applications, and numerical methods, *Journal of Soviet Mathematics* **64**, 783 (1993).

[77] J. Asbóth, L. Oroszlány, and A. Pályi, *A Short Course on Topological Insulators: Band Structure and Edge States in One and Two Dimensions*, Lecture Notes in Physics (Springer International Publishing, 2016).

[78] E. Jarlebring, W. Michiels, and K. Meerbergen, A linear eigenvalue algorithm for the nonlinear eigenvalue problem, *Numerische Mathematik* **122**, 169 (2012).

[79] T. Yoshida, T. Isobe, and Y. Hatsugai, Exceptional points and non-Hermitian skin effects under nonlinearity of eigenvalues, *Phys. Rev. B* **111**, 064310 (2025).

[80] S. Lieu, Topological phases in the non-Hermitian Su-Schrieffer-Heeger model, *Phys. Rev. B* **97**, 045106 (2018).

[81] J. H. Song, M. Maier, and M. Luskin, Nonlinear eigenvalue problems for coupled helmholtz equations modeling gradient-index graphene waveguides, *Journal of Computational Physics* **423**, 109871 (2020).

[82] E. Smolkin and Y. Smirnov, Numerical Study of the Spectrum of TE-Polarized Electromagnetic Waves of a Goubau Line Coated with Graphene, *Photonics* **10**, 1297 (2023).

[83] A. El Hassan, F. K. Kunst, A. Moritz, G. Andler, E. J. Bergholtz, and M. Bourennane, Corner states of light in photonic waveguides, *Nature Photonics* **13**, 697 (2019).

[84] Y. Yang, C. Roques-Carmes, S. E. Kooi, H. Tang, J. Beroz, E. Mazur, I. Kaminer, J. D. Joannopoulos, and M. Soljačić, Photonic flatband resonances for free-electron radiation, *Nature* **613**, 42 (2023).

[85] E. Slootman, W. Cherifi, L. Eek, R. Arouca, E. J. Bergholtz, M. Bourennane, and C. M. Smith, Breaking and resurgence of symmetry in the non-Hermitian Su-Schrieffer-Heeger model in photonic waveguides, *Phys. Rev. Res.* **6**, 023140 (2024).

[86] Z. Lin, W. Song, L.-W. Wang, H. Xin, J. Sun, S. Wu, C. Huang, S. Zhu, J.-H. Jiang, and T. Li, Observation of Topological Transition in Floquet Non-Hermitian Skin Effects in Silicon Photonics, *Phys. Rev. Lett.* **133**, 073803 (2024).

[87] W. Song, W. Sun, C. Chen, Q. Song, S. Xiao, S. Zhu, and T. Li, Breakup and Recovery of Topological Zero Modes in Finite Non-Hermitian Optical Lattices, *Phys. Rev. Lett.* **123**, 165701 (2019).

[88] A. Chaigne, Structural acoustics and vibrations, in *Springer Handbook of Acoustics*, edited by T. D. Rossing (Springer New York, New York, NY, 2014) pp. 941–1000.

[89] S. Liu, W. Deng, X. Huang, J. Lu, M. Ke, and Z. Liu, Robust Acoustic Waveguide Transport in Heterostructures Based on Acoustic Topological Insulators, *Phys. Rev. Appl.* **18**, 034066 (2022).

[90] J. Du, T. Li, X. Fan, Q. Zhang, and C. Qiu, Acoustic Realization of Surface-Obstructed Topological Insulators, *Phys. Rev. Lett.* **128**, 224301 (2022).

[91] Z.-G. Chen, W. Zhu, Y. Tan, L. Wang, and G. Ma, Acoustic Realization of a Four-Dimensional Higher-Order Chern Insulator and Boundary-Modes Engineering, *Phys. Rev. X* **11**, 011016 (2021).

[92] H. Xue, D. Jia, Y. Ge, Y.-j. Guan, Q. Wang, S.-q. Yuan, H.-x. Sun, Y. D. Chong, and B. Zhang, Observation of Dislocation-Induced Topological Modes in a Three-Dimensional Acoustic Topological Insulator, *Phys. Rev. Lett.* **127**, 214301 (2021).

[93] H. Xue, Y. Ge, H.-X. Sun, Q. Wang, D. Jia, Y.-J. Guan, S.-Q. Yuan, Y. Chong, and B. Zhang, Observation of an acoustic octupole topological insulator, *Nature Communications* **11**, 2442 (2020).